JCTC Journal of Chemical Theory and Computation

Article

pubs.acs.org/JCTC

On the Performance of Optimally Tuned Range-Separated Hybrid Functionals for X-ray Absorption Modeling

Paulo Cabral do Couto, Daniel Hollas, and Petr Slavíček*

Department of Physical Chemistry, University of Chemistry and Technology, Prague, Technická 5, Prague 6, 16628, Czech Republic

Supporting Information

ABSTRACT: We investigate the performance of optimally tuned range-separated hybrid functionals (OT-RSH) for modeling X-ray absorption spectra (XAS) of a benchmark set of simple molecules (water, ammonia, methane, hydrogen peroxide, hydrazine, and ethane), using time-dependent density functional theory (TDDFT). Spectra were simulated within the Path Integral based Reflection Principle methodology. Relative intensities, peak positions, and widths were compared with available experimental data. We show that the OT-RSH approach outperforms empirically parametrized functionals in terms of relative peak positions and intensities. Furthermore, we investigate the effect of geometry specific tuning where the range separation parameter is optimized for each geometry. Finally, we propose a simple correction scheme allowing for calculations of XAS on the absolute energy scale using the OT-RSH approach combined with ΔSCF/TDDFT-based calculations of core ionization energies.

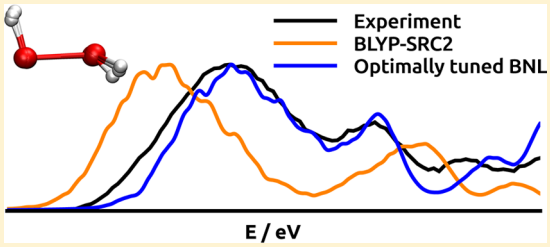

1. INTRODUCTION

Time-dependent density functional theory (TDDFT) has steadily become a primary tool for the description of valence electronically excited states.[1,2] Indeed, due to its computational efficiency, TDDFT is often the only feasible option for simulations of UV absorption spectra in realistic chemical systems.[3−6] More recently, the scope of TDDFT has been extended toward X-ray absorption spectroscopy (XAS).[7−10] While the performance of TDDFT has been thoroughly evaluated for the description of valence excited states,[11] the corresponding studies for core excited states are comparatively scarce.[12−17]

There are well-known limitations of TDDFT.[1,2,4] For instance, local or semilocal exchange-correlation functionals are known to fail for the description of delocalized,[18] charge-transfer,[19] and Rydberg[20] excited states. These failures mainly stem from the approximate nature of the exchange-correlation potential and the associated self-interaction error.[4,21,22] Shortcomings arising from electron self-interaction are usually mitigated through the admixture of exact (Hartree−Fock, HF) exchange within global[23] or range-separated[24−26] (RSH) hybrid functionals. In particular, the combination of long-range exact exchange and short-range semilocal exchange in RSH functionals provides reasonably accurate excitation energies for valence, Rydberg, and charge-transfer excited states.[11,27]

Within TDDFT, the description of core excited states presents a harder challenge than their valence counterpart as most of the self-interaction error is associated with strongly localized core electrons.[28] The resulting destabilization of core orbitals in common functionals leads to a consistent underestimate of the core excitation energies. This problem is usually tackled by the admixture of a large fraction of (short-range) exact exchange in global,[17] K and L shell specific,[12,13] range-separated[15−17] hybrid approaches or via *a posteriori* corrections.[29−31] None of the above hybrid approaches are fully general as the optimal fraction of exact exchange and range separation parameters depends on the particular system under consideration, e.g., on the atomic number of the nuclei.[17] Furthermore, we may ask what price do we pay for correct absolute core excitation energies. While a large fraction of global or short-range exact exchange is required for the accurate description of core orbitals,[17] the admixture of full long-range exact exchange and the associated correct asymptotic behavior of the exchange-correlation functional is vital for an accurate description of valence orbitals.[27] Finding a proper trade-off between these two requirements is far from trivial.

In this work, we adopt a different perspective. The failure to predict accurate absolute excitation energies is not a major flaw for the interpretation of XAS experiments as long as *relative* peak positions and intensities are correct. The calculated XAS can be simply shifted to match experiment or ΔSCF calculations for a reference low-lying excited state (*vide infra*). Since relative peak positions and intensities are mainly determined by the quality of unoccupied orbitals, methods that provide accurate excitation energies in the valence space[27,32] should also provide satisfactory results for XAS. To this end, we test the recently introduced optimally tuned range-separated hybrid approach as described below.[32]

Conventional global or range-separated hybrid functionals are usually empirically parametrized; i.e., the fraction of the HF exchange and/or range separation parameters are optimized to reproduce the properties of interest for a representative

Received: January 23, 2015

DOI: 10.1021/acs.jctc.5b00066
J. Chem. Theory Comput. XXXX, XXX, XXX−XXX

molecular training set.[17,26,33] However, it is well-known that the fraction of HF exchange and/or optimal range separation parameters are system-dependent.[17,32] Invoking the so-called IP theorem,[34−36] the optimal value for the range separation parameter (γ) of an N-electron molecule can be found *ab initio* by enforcing the condition that the HOMO orbital energy ($\varepsilon_{\mathrm{HOMO}}$) equals the negative of the first vertical ionization energy

$$\varepsilon_{\mathrm{HOMO}}(N,\gamma) = -IE_{\mathrm{HOMO}} = E(N,\gamma) - E(N-1,\gamma) \tag{1}$$

Range separation tuning can also, in principle, involve the IP theorem for corresponding anions. The RSH functionals for which eq 1 is enforced (optimally tuned RSHs, OT-RSH) provide not only accurate outer valence orbital energies and the corresponding ionization energies[32,37] but also superior energy gaps, absorption spectra, and response properties.[32,38−42] This indicates that both valence occupied and virtual orbitals are reliably described within the OT-RSH approach. The concept of range parameter tuning can be extended so that the optimization is performed for each orbital independently.[43,44]

Here, we present results for TDDFT simulated XAS spectra for a set of simple molecules (water, ammonia, methane, hydrogen peroxide, hydrazine, and ethane). We use the Baer−Neuhauser−Livshits[32] (BNL) functional as a representative of the RSHs. The results are compared both with experimental spectra and with spectra simulated with the BH$^{0.58}$LYP[17] and BLYP-SRC2[17] functionals, which were specifically designed for the description of core excited states.

In order to test the performance of the functionals for a wide range of molecular geometries, we have simulated the full band shapes of the XAS. The band shapes can be simulated conveniently for systems with bound excited states via evaluation of Franck−Condon integrals.[45] However, this is not possible for dissociative excited states. Therefore, we employed here a Path Integral Molecular Dynamics[46] based Reflection Principle (RP-PIMD)[47−49] approach. In this way, fluctuations due to thermal and vibrational motions are considered, which can be important in the XAS spectroscopy.[50,51]

The aim of this paper is threefold. First, we evaluate the general performance of the OT-RSH for the description of core excited states within TDDFT. We optimize the range separation parameter for each molecule in its equilibrium geometry (a *system specific*, SS-OT-RSH).

Second, we further improve the simulation protocol using a *geometry specific* optimal tuning approach (GS-OT-RSH). As simulations of XAS spectra within RP-PIMD involve averaging over a large number of configurations, structural fluctuations around the equilibrium geometry may significantly change core and valence orbital energies.[52] It is thus expected that *different* range separation parameters might be found for *different* configurations of the *same* system. Therefore, we investigate whether the geometry specific tuning is required for accurate modeling of XAS spectral features.

Finally, in the spirit of previous works,[50,53] we propose a simple, yet reliable, method for the correction of OT-RSH core excitation energies, based on the difference between ΔSCF- and TDDFT-based core ionization energies. It is shown that XAS calculated in this way can be quantitatively compared with experiment.

2. COMPUTATIONAL DETAILS

2.1. Simulation of XAS Spectra. X-ray absorption spectra were modeled within the Reflection Principle approximation,[47−49] in which the ground state density multiplied by the dipole strength is reflected onto the excited state and further on the energy axis:

$$\sigma(E) = \frac{\pi E}{3\hbar\varepsilon_0 c}\sum_b \int \varrho_a |\vec{\mu}_{ab}|^2 L(E - E_{ab})\mathrm{d}\vec{R} \tag{2}$$

Here, ϱ_a is the nuclear density distribution in the ground state, $\vec{\mu}_{ab}$ is the transition dipole moment in geometry $\vec{R}$, and E_{ab} is the difference between the excited and ground state electronic energies in the geometry $\vec{R}$ (semiclassical coordinate space approximation).[48] The function $L(E - E_{ab})$ is a delta function in the context of UV spectroscopy. The Reflection Principle then accounts for configurational broadening of the spectrum. However, core excited states have a finite lifetime, which is accounted for via the Lorentzian shape of the $L(E - E_{ab})$ factor

$$L(E - E_{ab}) = \frac{1}{\pi}\frac{\frac{\hbar}{2\tau}}{(E - E_{ab})^2 + \left(\frac{\hbar}{2\tau}\right)^2} \tag{3}$$

where τ is the lifetime of the core excited state, here taken as $\tau_{\mathrm{O}1s}$ = 3.6 fs, $\tau_{\mathrm{N}_{1s}}$ = 4.7 fs, and $\tau_{\mathrm{C}_{1s}}$ = 7.8 fs.[54] Lifetimes are assumed to be the same for the same atoms in different molecules, and variation for different electronic states is neglected. Note that the Reflection Principle accounts for non-Condon effects as the transition dipole moment is calculated for each geometry. On the other hand, it only provides a low resolution spectrum without the vibrational progression.

The critical parameter controlling the quality of the simulation is the ground state density ϱ_a.[48,49,51,55] Here, we adopted a Path Integral Molecular Dynamics[46] approach combined with a quantum thermostat based on the Generalized Langevin Equation (PI+GLE method).[56,57] This method converges quickly to the quantum limit with respect to the number of beads; only 4 beads are typically needed for accurate position distributions.[57] Energies and gradients in the ground state were calculated using the PBE[58,59] exchange-correlation functional with the aug-cc-pVDZ[60,61] basis set. Simulations were run with a time step of 20 au for 98 000 steps, after 2000 initial thermalization steps. Temperature was kept at 298 K. A total of 800 uncorrelated configurations were sampled and used in subsequent calculations. The PI+GLE simulations were carried out with the in-house ABIN code.[62] Energies and gradients were calculated using the Gaussian 09 program.[63]

Comparison of simulated spectra with experiment is not trivial because experimental cross sections are not available and each theoretical method yields simulated spectra that differ in intensity and energy ranges. It is, therefore, necessary to devise an unbiased approach where peak intensities, peak positions, and widths can be compared unambiguously. The present approach is based on the maximization of the overlap I between simulated and experimental spectra. The latter is taken as the reference spectrum after the area of the corresponding curve is normalized to unity. The calculated spectrum is then transformed with two parameters. The energy scale is shifted by β_t, and for each β_t the spectrum is scaled as to normalize the spectrum between the experimental onset of absorption (E_0) and core ionization threshold E_{IE}. We then maximize the overlap integral depending on these two parameters

$$I(\alpha_t,\beta_t) = \int_{E_0}^{E_{IE}} \alpha_t\sigma_t(E + \beta_t)\sigma_r(E)\mathrm{d}E \tag{4}$$

DOI: 10.1021/acs.jctc.5b00066
J. Chem. Theory Comput. XXXX, XXX, XXX−XXX

where $\sigma_t(E)$ and $\sigma_r(E)$ are the absorption cross sections of the simulated and normalized reference cross sections at energy E. Maximization of $I(\alpha_t, \beta_t)$ under the constraint of normalization and within appropriate bounds for β_t thus yields optimal intensity and energy scale factors. Direct comparison with experiment can be carried out using the scaled and shifted spectra or only the scaled spectra with the scaling parameter calculated with the optimal β_t.

Peak positions and full width at half-maximum (FWHM) were estimated through nonlinear fitting using the Fityk program.[64]

2.2. Calculations of Core Excited States. Core excitation energies and associated intensities were calculated using TDDFT within the Tamm−Damcoff approximation.[65] An efficient computational approach to the calculation of core excited states was achieved by restricting the occupied space to the prescribed core orbital.[3,17] No restrictions were imposed on the virtual space. Calculations were carried out using a 100 point Euler−Mclaurin radial grid with 302 point Lebedev angular grid.

The BNL[32,66,67] functional was taken as a representative of a long-range corrected RSH functionals. This functional is based on a combination of long-range exact (nonlocal) and Slater local exchange with the LYP correlation functional. The range separation parameter was optimized either for experimental gas phase equilibrium geometries[68] (γ_{eq}) or for each sampled configuration (γ_{opt}).

The BH$^{0.58}$LYP and BLYP-SRC2[17] functionals were taken as representatives of empirically parametrized functionals geared toward the prediction of core excitations of valence and Rydberg character. Here, common functionals are expected to fail within the TDDFT framework (while other DFT-based approaches still might work[50,51,69]). The BH$^{0.58}$LYP is a three-parameter global hybrid functional in the same functional form as B3LYP,[23] with a larger (58%) fraction of Hartree−Fock exchange. The BLYP-SRC2 is a short−range corrected RSH with an admixture of exact exchange in the short- (C_{SHF} = 0.55, μ_{SR} = 0.69 a_0^{-1}) and long- (C_{LHF} = 0.08, μ_{LR} = 1.02 a_0^{-1}) range regimes.[17]

All TDDFT calculations utilized the 6-311(2+, 2+)G(d,p)[70,71] basis set and were carried out using the Q-Chem4.1[72] program.

2.3. Correction for the Absolute Energies. TDDFT typically exhibits large deviations of XAS excitation energies on the absolute scale. These deviations are expected to be mostly associated with core electron self-interaction.[28] For each sampled geometry, the deviation ΔIE_{1s} can be equivalently expressed as an error of TDDFT core ionization energy relative to accurate reference theoretical values:

$$\Delta IE_{1s} = IE_{1s}^{\mathrm{MOM}} + \Delta E_{\mathrm{rel}} - IE_{1s}^{\mathrm{TDDFT}} \quad (5)$$

The reference core ionization energy IE_{1s}^{MOM} is determined here via the Maximum Overlap Method[73] (MOM) with a further correction for relativistic effects (ΔE_{rel}). The MOM method provides self-consistent approximations to excited states by maximizing the overlap between the excited-state determinants of successive self-consistent field iterations. The reference MOM core ionization energies were calculated at the RI-MP2[74] and RI-CCSD[75] theory levels. The TDDFT-based core ionization energies (IE_{1s}^{TDDFT}) were calculated as a difference of the total energy of the lowest core excited ionic state and the ground state energy of the neutral molecule, which can be equivalently expressed as

$$IE_{1s}^{\mathrm{TDDFT}} = IE_{\mathrm{HOMO}} + E_{\mathrm{exc}}(1s \rightarrow \mathrm{SOMO}) \quad (6)$$

which is the sum of the first ionization energy (IE_{HOMO}) and the lowest core excitation energy of the valence ionized molecule ($E_{\mathrm{exc}}(1s \rightarrow \mathrm{SOMO})$).

The relativistic correction (ΔE_{rel}) associated with the removal of one electron from a core 1s orbital was estimated as a difference of relativistic and nonrelativistic core orbital energies at the Hartree−Fock level of theory. The Douglas−Kroll−Hess Hamiltonian with first-order spin−orbit and second-order scalar relativistic effects[76] was used for relativistic calculations. The relativistic corrections for H_2O (0.41 eV), NH_3 (0.23 eV), and CH_4 (0.12 eV) were assumed to be geometry-independent, and the same values were also used for H_2O_2, N_2H_4, and C_2H_6 analogues. It should be noted that the empirical parametrization of the BH$^{0.58}$LYP and BLYP-SRC2 for molecules containing first row atoms includes an implicit account of relativistic effects.

All the calculations were carried out with the 6-311(2+,2+)G(d,p) basis set.[70,71] Calculations of ΔE_{rel} were carried out with the uncontracted 6-311(+,+)G(d,p) basis set.[70,71]

MOM calculations were carried out using the Q-Chem4.1 program.[72] Calculations of ΔE_{rel} were carried out with the Dirac2012 program.[77]

3. RESULTS AND DISCUSSION

The assessment of the OT-RSH is based on a test set of six molecules for which reliable experimental X-ray absorption spectra could be found: H_2O,[78] NH_3,[78] CH_4,[79] H_2O_2,[80] N_2H_4,[81] and C_2H_6.[82] The first row H_2O, NH_3, and CH_4 hydrides were taken as model systems to determine whether OT-RSHs accurately describe XAS for stiff systems with a single heavy atom. Flexible molecules with two heavy centers (H_2O_2, N_2H_4, and C_2H_6) were also considered to investigate the effects of geometry variations. Before we discuss the various aspects of the RSHs, we briefly review the character of the electronic transitions from the 1s orbital in the above molecules.

Water and ammonia are isoelectronic molecules with a rather similar electronic structure. The experimental X-ray absorption spectra of both molecules are comparable;[78] the two lowest energy absorption bands involve transitions from the 1s orbital into the LUMO and LUMO+1 orbitals, which correspond to a combination of σ^* orbitals with 3s and 3p Rydberg orbitals. Higher energy excitations correspond to transitions to higher Rydberg orbitals.

The experimental gas phase X-ray absorption spectrum of hydrogen peroxide is characterized by a broad peak involving transitions to the σ^*(O−O) orbital and a narrower peak corresponding to transitions to doubly degenerate σ^*(O−H) orbitals.[80] In contrast, the gas phase X-ray absorption spectrum of hydrazine is characterized by two low energy peaks involving transitions into 3s Rydberg orbitals and σ^*(N−H) orbitals, respectively.[81] The higher energy broad peak involves transitions to the σ^*(N−N) orbital.[81]

The experimental gas phase X-ray absorption spectrum of methane lacks clearly identifiable transitions of valence character.[78,83] Main features are assigned to Rydberg transitions, where the lowest energy and weak intensity band corresponds to the dipole-forbidden transition to the 3s Rydberg orbital, only visible through coupling to vibrational modes of t_2 symmetry.[83] The dominant peak corresponds to the transition from the 1s orbital into the 3p Rydberg orbital. Higher energy peaks correspond to transitions to higher Rydberg states. Similarly to methane, the experimental gas phase X-ray absorption spectrum of ethane[84] is characterized by a strong absorption band corresponding to the transition to the 3p Rydberg orbital

DOI: 10.1021/acs.jctc.5b00066
J. Chem. Theory Comput. XXXX, XXX, XXX−XXX

Table 1. Calculated and Experimental Excitation Energies E (in eV) and Oscillator Strengths for the H_2O, NH_3, and CH_4 Molecules in Their Gas Phase Equilibrium Geometries. Results for the Mean Absolute Deviation from Experiment (MAD) for Excitation Energies for All Core Excitations (all), Core Excitations into Valence States (val), Core Excitations into Rydberg States (ryd), and Relative Excitation Energies (rel) Are Presented[a]

	BLYP		B3LYP		CAM-B3LYP		LRC-BLYP		BNL(γ_{eq})		EOM-CCSD		exp.
	E	f	E	f	E	f	E	f	E	f	E	f	
H_2O													
$O_{1s} \rightarrow 4a_1/3s$	510.0	0.004	518.5	0.008	518.6	0.008	510.5	0.005	507.8	0.007	535.7	0.013	534.0
$O_{1s} \rightarrow 2b_2/3p$	511.1	0.002	520.0	0.011	520.2	0.013	512.2	0.010	509.6	0.018	537.5	0.026	535.9
NH_3													
$N_{1s} \rightarrow 4a_1/3s$	379.8	0.002	387.3	0.004	387.4	0.004	380.5	0.003	378.0	0.003	402.1	0.006	400.7
$N_{1s} \rightarrow 2b_2/3p$	380.7	0.002	388.5	0.007	388.8	0.009	382.0	0.008	379.6	0.013	403.8	0.019	402.3
CH_4													
$C_{1s} \rightarrow 3s$	268.6	0.000	275.0	0.000	275.3	0.000	269.6	0.000	267.8	0.000	287.8	0.000	286.9
$C_{1s} \rightarrow 3p$	269.2	0.001	275.9	0.004	276.3	0.006	270.7	0.005	269.1	0.009	289.1	0.013	288.0
MAD (all)	21.41		13.75		13.54		20.37		22.66		1.37		
MAD (val)	22.84		14.64		14.46		21.91		24.50		1.55		
MAD (ryd)	18.56		11.98		11.68		17.29		19.01		1.02		
MAD (rel)	0.66		0.34		0.21		0.10		0.09		0.12		

[a]The 6-311(2+2+)G(d,p) basis set was used throughout. Experimental data were taken from refs 78 and 79.

centered at ∼288 eV. The dipole-forbidden transition from HOMO orbitals to the 3*s* Rydberg orbitals gives rise to a shoulder at ∼287 eV.

3.1. Performance of Optimally Tuned Functionals for XAS Modeling. *Initial Considerations.* The present work rests on the hypothesis whether optimally tuned range-separated hybrids provide accurate relative core excitation energies. The correction of TDDFT excitation energies for the absolute energy scale is discussed in the next section. We, therefore, focus on the structure of the spectrum, i.e., on relative energies and intensities.

As a first test of the performance of the present approach, the BLYP functional and related global and range separated hybrid functionals are evaluated. Table 1 shows results for TDDFT core excitation energies and oscillator strengths for a single heavy atom molecule test set. As expected and well-documented, TDDFT core excitation energies deviate significantly from experiment for all functionals. On the other hand, the comparison of the errors for relative energies shows that range-separated hybrids with full exact long-range exchange yield the most accurate results. While the EOM-CCSD method outperforms all the functionals discussed above for absolute energies, range-separated hybrids with full exact long-range exchange are equally accurate for relative energies. Note that oscillator strengths for optimally tuned BNL are the closest to those of EOM-CCSD.

System vs Geometry Specific Tuning of the Range Separation Parameter. The initial screening suggested that the OT-RSH might constitute a useful tool for XAS modeling. We, therefore, proceeded with the simulation of full BNL XAS spectra within the Reflection Principle that allows a direct comparison with experiment. Experimental and calculated XAS spectra are compared in Figure 1. Note that simulated spectra are scaled and shifted to maximize the overlap with experiment.

Two different strategies for the optimization of the range separation parameter are considered. In the first one, the range separation parameter was optimized for each molecule in its equilibrium geometry (BNL(γ_{eq})). However, changes in molecular structure are necessarily accompanied by changes in electronic structure, particularly when highly distorted geometries are sampled from classical or quantum molecular dynamical simulation. It is, therefore, natural to question whether range parameter tuning at a single geometry (system specific approach − SS-OT-RSH) is transferable to geometries far from equilibrium. In fact, geometry specific tuning (GS-OT-RSH) was recently shown to provide simultaneously accurate geometries, vibrational modes, and valence orbital energies for the G2 data set.[85] In the second optimization strategy, we optimized the range separation parameter for each geometry (BNL(γ_{opt})). We address two questions: (i) what is the general performance of the range separated hybrid functionals for the XAS simulations and (ii) do reliable simulations of the experimental spectra via the Reflection Principle require determination of an optimal range separation parameter for *each* sampled geometry (γ_{opt})?

The general conclusion extracted from Figure 1 is that optimally tuned BNL functionals provide an excellent estimate of the structure of the spectra, i.e., relative peak positions and intensities along with peak widths. For instance, the BNL functional reproduces all spectral features of water XAS. While the experimental shapes of the spectra are typically well-reproduced by our simulations, there is a noticeable exception—the CH_4 molecule. The excited states of Rydberg character lead to a relatively narrow spectrum with a vibrational resolution. Such phenomena cannot be described within the Reflection Principle approach. However, the calculated spectrum of methane still closely follows experimental patterns and the modeled spectrum and is in fact in good agreement with EELS experimental results by Hitchcock et al.[86]

To make our conclusions quantitative, we have extracted the positions, intensities, and widths for different peaks; the results are summarized in Table 2. The overall error for the peak centers is just 0.11 eV, reflecting a very good description of the relative peak positions.

Figure 1 and Table 2 also illustrate the difference between the SS-OT-RSH and GS-OT-RSH approaches. Relative intensities and peak widths, including the O1$s \rightarrow 3p$ Rydberg transition, are in better agreement for the BNL(γ_{opt}) approach for water and hydrogen peroxide. Generally, the GS-OT-RSH approach leads to broader peaks. No significant differences are observed for ammonia and hydrazine, which can be rationalized by a narrower

DOI: 10.1021/acs.jctc.5b00066
J. Chem. Theory Comput. XXXX, XXX, XXX−XXX

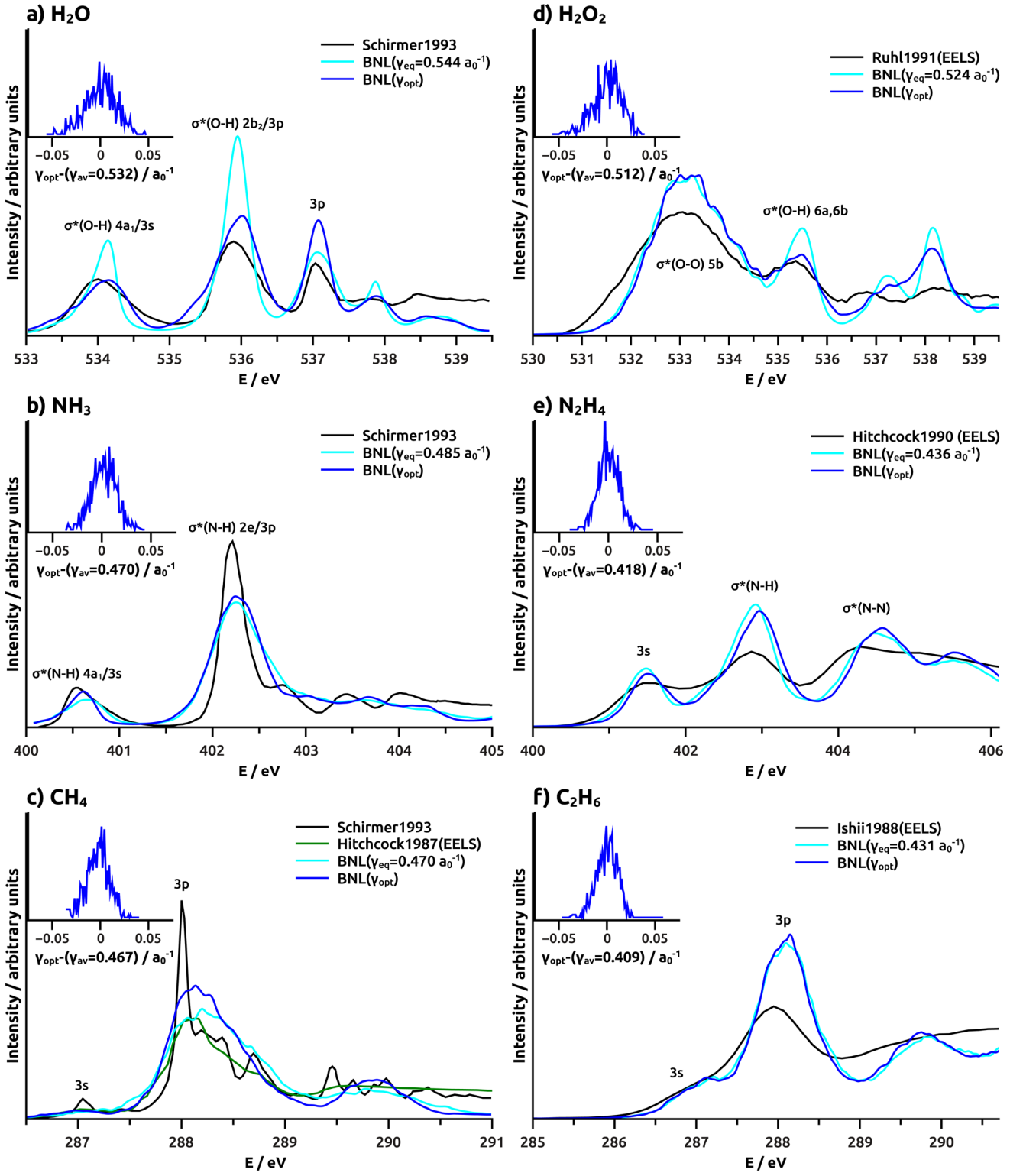

Figure 1. Experimental (black) and simulated BNL(γ_{eq}) (light blue) and BNL(γ_{opt}) (blue) X-ray absorption spectra for six model molecules. Simulated spectra are scaled under the constraint of normalization and shifted to maximize the overlap with experiment.

distributions of the γ_{opt} parameter for NH_3 and N_2H_4 relative to those of H_2O and H_2O_2 (see insets in Figure 1). In the case of methane and ethane, there are also slight differences between the GS-OT-RSH and SS-OT-RSH methods, but they are rather small compared to the limitations of the Reflection Principle.

The SS-OT-RSH and GS-OT-RSH approaches lead to spectra with different intensities, particularly for the water molecule. It should be noted that the different intensity stems from different peak widths for the two methods; the integrated intensity is approximately the same for both SS-OT-RSH and GS-OT-RSH (for unscaled spectra). In other words, the variations in the γ parameter affect the oscillator strengths only weakly.

To summarize, the comparison of the BNL(γ_{eq})- and BNL(γ_{opt})-based spectra with experiment shows that the SS-

DOI: 10.1021/acs.jctc.5b00066
J. Chem. Theory Comput. XXXX, XXX, XXX−XXX

Table 2. Parameters of Simulated Spectra Using BNL(γ_{eq}) and BNL(γ_{opt}) and Comparison with Experiment. The Peak Centers and FWHMs Are Provided in eV[a]

	BNL(γ_{eq})			BNL(γ_{opt})			experiment		
	center	height	FWHM	center	height	FWHM	center	height	FWHM
H_2O									
$O_{1s} \rightarrow 4a_1/3s$	534.16	0.38	0.41	534.16	0.21	0.75	533.98	0.23	0.90
$O_{1s} \rightarrow 2b_2/3p$	535.96	0.81	0.40	535.99	0.48	0.72	535.86	0.37	0.47
$O_{1s} \rightarrow 3p$	537.09	0.59	0.59	537.08	0.44	0.38	537.02	0.26	0.12
NH_3									
$N_{1s} \rightarrow 4a_1/3s$	400.67	0.18	0.51	400.62	0.23	0.29	400.51	0.25	0.45
$N_{1s} \rightarrow 2b_2/3p$	402.24	0.81	0.70	402.26	0.86	0.64	402.20	1.21	0.30
CH_4									
$C_{1s} \rightarrow 3s$	287.14	0.03	0.34	287.03	0.04	0.45	287.01	0.09	0.41
$C_{1s} \rightarrow 3p$	288.14	0.70	1.02	288.08	0.86	0.67	288.01	1.37	0.14
H_2O_2									
$O1s \rightarrow \sigma^*(O-O)$	533.04	0.26	2.01	533.08	0.26	1.93	533.02	0.20	2.37
$O1s \rightarrow \sigma^*(O-H)$	535.52	0.14	0.63	535.48	0.09	0.85	535.40	0.10	1.24
N_2H_4									
$N1s \rightarrow 3s$	401.48	0.16	0.49	401.52	0.14	0.52	401.48	0.20	1.39
$N1s \rightarrow \sigma^*(N-H)$	402.91	0.39	0.72	402.98	0.37	0.78	402.91	1.20	0.92
$N1s \rightarrow \sigma^*(N-N)$	404.48	0.29	1.07	404.54	0.31	0.99	404.17	2.20	0.96
C_2H_6									
$C1s \rightarrow 3s$	287.07	0.11	0.53	287.06	0.12	0.39	287.02	0.07	0.84
$C1s \rightarrow 3p$	288.10	0.57	0.84	288.11	0.59	0.78	287.91	0.26	0.85
MAD (all)	0.11	0.38	0.36	0.11	0.32	0.30			
MAD (val)	0.12	0.52	0.34	0.14	0.41	0.24			
MAD (ryd)	0.10	0.24	0.44	0.07	0.19	0.37			

[a]The spectra were scaled under the constraint of normalization and shifted to maximize the overlap with experimental spectra (see Figure 1). The relative heights were taken from the normalized spectra. Experimental data were taken from refs 78−82.

Table 3. Calculated and Experimental Excitation Energies (in eV) for the H_2O, NH_3, and CH_4 Molecules in Their Gas Phase Equilibrium Geometries. Oscillator Strengths Are Presented in Parentheses. Results for the Maximum Absolute Deviation Relative to Experiment (MAD) for All Excitation Energies (E_{all}), Core Excitations into Valence (E_{val}), and Rydberg States (E_{ryd}) along with Relative Excitation Energies (E_{rel}) Are Also Presented[a]

	BNL(γ_{eq} + ΔIE_{1s})						
	BNL(γ_{eq})	RI-MP2	RI-CCSD	f	$BH^{0.58}LYP$	BLYP-SRC2	exp.
H_2O							
$O_{1s} \rightarrow 4a_1/3s$	527.8	534.4	534.2	(0.007)	534.5 (0.020)	534.3 (0.016)	534.0
$O_{1s} \rightarrow 2b_2/3p$	529.6	536.2	536.0	(0.018)	535.9 (0.043)	535.7 (0.030)	535.9
NH_3							
$N_{1s} \rightarrow 4a_1/3s$	395.4	401.1	400.9	(0.003)	401.4 (0.010)	401.2 (0.007)	400.7
$N_{1s} \rightarrow 2b_2/3p$	397.0	402.7	402.6	(0.013)	402.6 (0.040)	402.5 (0.019)	402.3
CH_4							
$C_{1s} \rightarrow 3s$	282.8	287.5	287.4	(0.000)	287.1 (0.000)	287.2 (0.000)	286.9
$C_{1s} \rightarrow 3p$	284.0	288.7	288.7	(0.009)	288.1 (0.033)	288.1 (0.009)	288.0
MAD (E_{all})	5.21	0.51	0.31		0.39	0.28	
MAD (E_{val})	5.79	0.47	0.29		0.38	0.32	
MAD (E_{Ryd})	4.06	0.66	0.58		0.18	0.19	
MAD (E_{rel})	0.07	0.18	0.18		0.32	0.37	

[a]The 6-311(2+2+)G(d,p) basis set was used throughout. Experimental data were taken from refs 78 and 79.

OT-RSH approach already yields accurate results for the relative positions of absorption bands. However, the GS-OT-RSH approach leads to broader peaks if the system exhibits a broad distribution of γ_{opt}.

3.2. The Absolute Scale in XAS Simulations: *Ab Initio* vs Empirical Parametrization. For most of the general-purpose functionals, TDDFT core excitation energies deviate significantly from experimental data. For example, the first valence peak for water XAS presented in Figure 1 is shifted by ∼26 eV in the BNL(γ_{eq}) calculation. These deviations are well-understood in terms of the electron self-interaction, which destabilizes the core orbitals.

It should be noted that core excitation energies calculated with the same functional using the ΔSCF approach (here represented by the MOM method) agree better with experiment than those using TDDFT.[87] Taking the first excited state of water calculated

DOI: 10.1021/acs.jctc.5b00066
J. Chem. Theory Comput. XXXX, XXX, XXX−XXX

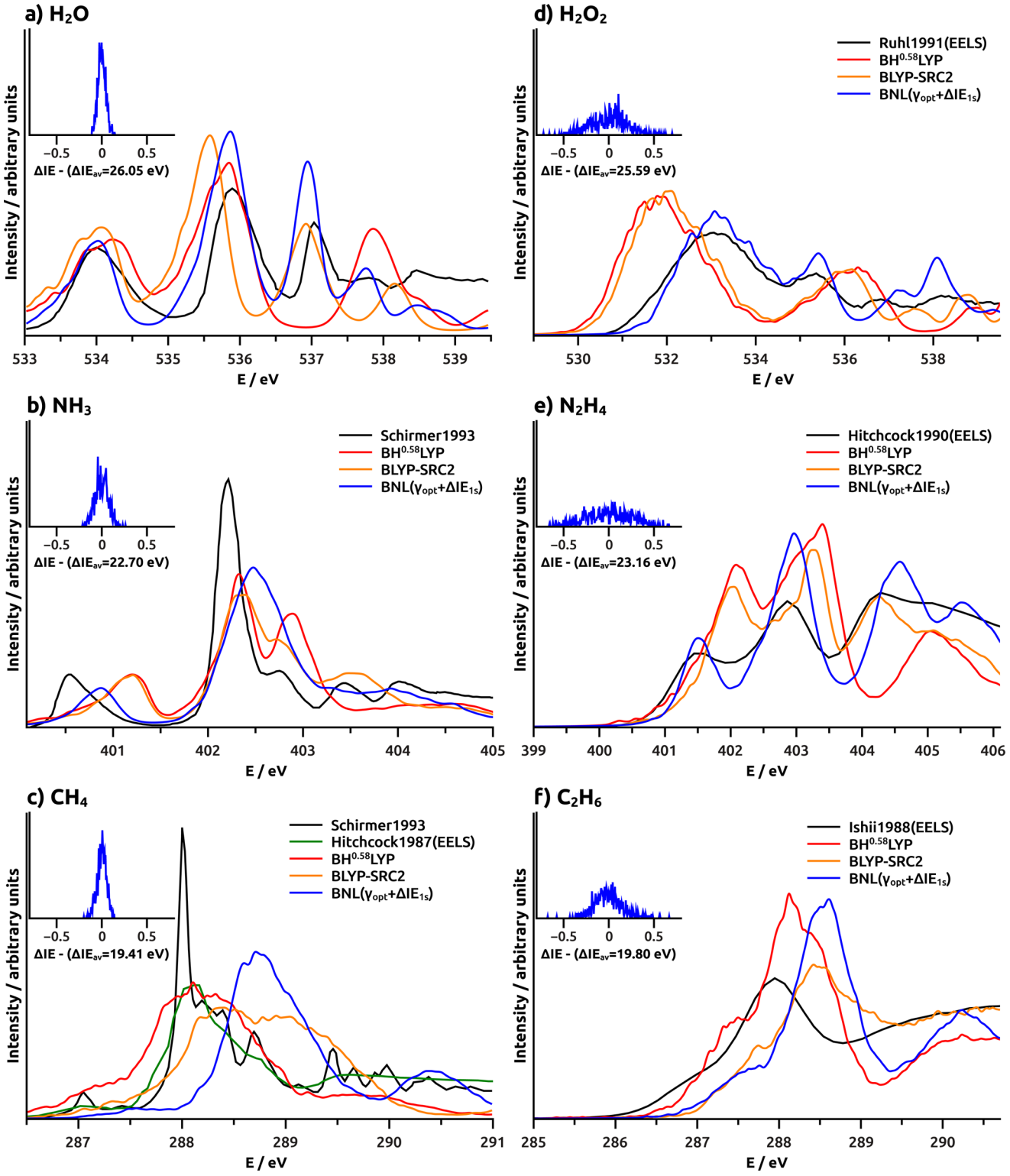

Figure 2. Experimental (black) and simulated BH$^{0.58}$LYP (red), BLYP-SRC2 (orange), and BNL(γ_{opt} + ΔIE_{1s}) (blue) X-ray absorption spectra. Spectra were scaled as described in the Computational Details section but not shifted. The distribution of the ΔE_{1s} corrections for different geometries is shown as insets.

with the B3LYP functional as an example, the MOM excitation energy is 533.8 eV, whereas the TDDFT excitation energy is 518.5 eV (experimental value is 534.0 eV). Although it was observed some time ago that valence ΔSCF and TDDFT excitation energies do not match,[8,88] the extent of the discrepancy for core excited states is rather surprising.[87] Range-separated hybrids provide inferior absolute excitation energies even within the MOM method. For water, we obtain 527.8 eV with the BNL(γ_{eq}) functional and the TDDFT energy is 507.6 eV.

Similar trends are observed for core ionization energies: ΔSCF ionization energies are reasonably accurate for common

DOI: 10.1021/acs.jctc.5b00066
J. Chem. Theory Comput. XXXX, XXX, XXX−XXX

Table 4. Parameters of Experimental and Simulated Spectra Using BNL(γ_{opt} + ΔIE_{1s}), BH$^{0.58}$LYP, and BLYP-SRC2 Functionals. The Peak Centers and FWHMs Are Provided in eV[a]

	BH$^{0.58}$LYP			BLYP-SRC2			BNL(γ_{opt} + ΔIE_{1s})			experiment		
	center	height	FWHM	center	height	FWHM	center	height	FWHM	center	height	FWHM
H_2O												
$O_{1s} \rightarrow 4a_1/3s$	534.23	0.22	1.03	534.10	0.25	0.91	534.02	0.24	0.69	533.98	0.23	0.90
$O_{1s} \rightarrow 2b_2/3p$	535.83	0.44	0.90	535.59	0.51	0.66	535.87	0.52	0.67	535.86	0.37	0.47
$O1s \rightarrow 3p$	537.85	0.28	0.74	536.92	0.29	0.61	537.02	0.42	0.39	537.02	0.26	0.12
NH_3												
$N_{1s} \rightarrow 4a_1/3s$	401.24	0.23	0.53	401.20	0.24	0.52	400.87	0.19	0.46	400.51	0.25	0.45
$N_{1s} \rightarrow 2b_2/3p$	402.33	0.65	0.39	402.33	0.60	0.38	402.49	0.77	0.75	402.20	1.21	0.30
CH_4												
$C_{1s} \rightarrow 3s$	287.10	0.13	0.68	287.45	0.04	0.67	287.53	0.03	0.39	287.01	0.09	0.41
$C_{1s} \rightarrow 3p$	288.11	1.15	1.15	288.28	0.40	0.71	288.70	0.82	0.82	288.01	1.37	0.14
H_2O_2												
$O_{1s} \rightarrow \sigma^*$(O−O)	531.67	0.27	2.10	531.85	0.28	2.09	533.01	0.23	2.18	533.02	0.20	2.37
$O_{1s} \rightarrow \sigma^*$(O−H)	536.32	0.13	1.76	536.13	0.13	1.53	535.44	0.12	0.76	535.40	0.10	1.24
N_2H_4												
$N_{1s} \rightarrow 3s$	402.13	0.24	0.90	401.99	0.12	0.72	401.60	0.12	0.72	401.48	0.20	1.39
$N_{1s} \rightarrow \sigma^*$(N−H)	403.41	0.37	1.15	403.31	0.33	0.89	403.04	0.33	0.89	402.91	1.20	0.92
$N_{1s} \rightarrow \sigma_*$(N−N)	405.05	0.18	1.36	404.26	0.27	1.46	404.66	0.27	1.46	404.17	2.20	0.96
C_2H_6												
$C_{1s} \rightarrow 3s$	287.42	0.24	0.77	287.71	0.12	0.64	287.57	0.10	0.87	287.02	0.07	0.84
$C_{1s} \rightarrow 3p$	288.15	0.55	0.90	288.42	0.33	0.40	288.57	0.55	0.80	287.91	0.26	0.85
MAD (all)	0.51	0.31	0.34	0.44	0.35	0.29	0.28	0.33	0.27			
MAD (val)	0.60	0.45	0.27	0.45	0.47	0.18	0.18	0.44	0.26			
MAD (ryd)	0.38	0.13	0.42	0.42	0.21	0.44	0.42	0.19	0.29			

[a]Spectra were scaled as described in the Computational Details section, but not shifted (see Figure 2). The relative heights were taken from the normalized spectra. Experimental data were taken from refs 78−82.

functionals and somewhat worse for the RSH functionals.[89] The low accuracy of the RSHs for the core electron ionization energies can be understood as the RSHs are optimized for valence orbital, which takes its toll in the core region. The ΔSCF energies are surprisingly not very accurate also for the short-range corrected BLYP-SRC2 functional,[89] suggesting that the good performance of this method for absolute TDDFT energies stems from error cancellation.

In practice, the shift in absolute energy does not represent a major hurdle for interpretation of experimental spectra. It would be, however, more satisfactory to use a protocol that would quantitatively predict excitation energies and peak positions. We can shift the spectra using the ΔSCF value for the lowest excitation or core electron binding energy. Such a correction can be made either with the DFT methods or more safely with more advanced electronic structure approaches.

In principle, the simplest correction would be to shift the spectra by the difference between high level *ab initio* and TDDFT excitation energies. However, the MOM does not necessarily lead to a well-defined excited state. Therefore, we chose a more robust approach, where the error associated with a given core orbital is estimated via the difference in core ionization energies. An accurate core ionization energy can be conveniently computed via the MOM combined with any standard high level electronic structure method such as MP2 or CCSD. We can also use many of the standard DFT functionals to provide the reference value of the core ionization energy.[89] The TD-DFT-based core ionization energy was computed via the core excitation of the ionized system (see the Computational Details section for details).

In Table 3, the performance of the BNL(γ_{eq} + ΔIE_{1s}) approach is evaluated for the two lowest core excitations of the H_2O, NH_3, and CH_4 molecules in their gas phase equilibrium geometries. Reference core ionization energies IE_{1s}^{MOM} were calculated through the MOM with the BNL, RI-MP2, and RI-CCSD electron structure methods and further corrected for relativistic effects. For a comparison, the core excited energies obtained with the BH$^{0.58}$LYP and BLYP-SRC2 functionals (with no additional correction) are also presented. Similar comparison for the H_2O_2, N_2H_4, and C_2H_6 molecules based on single geometry is problematic due to ambiguous assignment of the experimental peaks and problems associated with equivalent nuclei in symmetric structures.

Inspection of Table 3 shows that correcting the TDDFT excitation energies using the ΔSCF ionization energy calculated with the same functional does not yield very accurate results for the BNL functional. This is consistent with the poor performance of the RSHs for core ionization energies.[89] On the other hand, the use of MP2 or CCSD core ionization energies for the calculation of ΔIE_{1s} (eq 5) as a correction to the BNL(γ_{eq}) excitation energies leads to a very good agreement with experimental data. The corrected values are comparable to those obtained with the TDDFT using the BH$^{0.58}$LYP and BLYP-SRC2 functionals. The latter methods agree better for Rydberg transitions in the case of CH_4 and C_2H_6 molecules. However, the relative energy differences between valence excitations are in better agreement with experiment using the OT-RSH approach while they are consistently overestimated by the BH$^{0.58}$LYP and BLYP-SRC2 methods (see MAD(E_{rel}) in Table 3). Note that the correction scheme is consistent only when the IP theorem is fulfilled (see Figure SI1 in the Supporting Information).

DOI: 10.1021/acs.jctc.5b00066
J. Chem. Theory Comput. XXXX, XXX, XXX−XXX

Spectra simulated with the BNL(γ_{opt} + ΔIE_{1s}), BH$^{0.58}$LYP, and BLYP-SRC2 functionals are presented in Figure 2. The CCSD energies were used for the ΔIE_{1s} correction. For a quantitative analysis, we extracted the peak features for the different transitions via fitting the experimental and calculated spectra into a suitable functional form; the results are summarized in Table 4.

Visual inspection of Figure 2 and data in Table 4 shows that the BNL(γ_{opt} + ΔIE_{1s}) approach yields relative and absolute peak positions for valence transitions (Figure 2a,b,d,e) that are in very good agreement with experiment. The success of the OT-RSH approach is most evident for hydrogen peroxide, where the experimental spectrum is adequately reproduced. Relative peak intensities and shapes are also in good agreement with experiment, within the limitations of the Reflection Principle. On the other hand, both the BH$^{0.58}$LYP and BLYP-SRC2 empirical approaches do not agree satisfactorily with experiment with regard to absolute peak position (Figure 2d), peak shape, and relative intensities (Figure 2b,e). The shortcomings of an empirical approach are more apparent for relative peak positions, which are either overestimated (Figure 2d) or underestimated (Figure 2a,b).

The ΔIE_{1s} correction was calculated for each geometry as it is geometry-dependent (see insets in Figure 2); therefore, the shapes of the calculated spectra are slightly different with respect to the spectra presented in Figure 1. However, the differences between the BNL(γ_{opt} + ΔIE_{1s}) and BNL(γ_{opt}) spectra are small, with the exception of a slight improvement of the relative intensities of the second and third peaks in the water XAS. A simple rigid shift of the BNL(γ_{eq}) or BNL(γ_{opt}) spectra by a single ΔIE_{1s} correction provides comparable spectra at essentially no computational overhead.

We have so far ignored the absolute intensities during the assessment of different protocols for the XAS simulations, mainly due to the lack of reliable experimental data. However, it should be noted that absolute intensities of the transitions are strongly dependent on the functional (see Table 3). The differences are best seen in Figure SI2 (see the Supporting Information), in which the calculated spectra are presented with absolute intensities.

4. CONCLUSIONS

We tested the performance of optimally tuned long-range-separated functionals for the simulations of K-edge XAS spectra. The results were compared with available experimental data. For a comparison, we also simulated XAS with two empirically parametrized functionals specifically developed for a description of core excited states (global BH$^{0.58}$LYP and short-range corrected BLYP-SRC2 hybrid functionals). The comparison was based on a molecular test set comprising water, ammonia, methane, hydrogen peroxide, hydrazine, and ethane.

Our benchmarking was based on the inspection of full XAS, analyzing peak positions, band shapes, and intensities for different transitions. The X-ray absorption spectra were simulated using the Reflection Principle combined with the efficient PI+GLE method for generating the ground state density. In this way, the performance of the electronic structure methods was assessed even for highly distorted geometries.

Optimal tuning of the range parameter leads to a very good agreement between experimental and simulated XAS spectra with respect to the relative positions, relative intensities, and (within the limitations of the Reflection Principle) widths of the absorption peaks. While empirically parametrized functionals provided a fair estimate of the absolute positions of the excitation energies, the OT-RSH scheme better describes the structure of the spectrum.

We quantitatively compared the system and geometry specific OT-RSH. The results for core transitions into valence orbitals of water and hydrogen peroxide suggest that, in some cases, the GS-OT-RSH approach is required for a close agreement with experiment with regard to relative peak intensities and shapes. On the other hand, a geometry specific approach is computationally more demanding and the system specific optimization should, in most cases, provide a reliable estimate of the XAS spectral features.

The major weakness of the OT-RSH approach is a poor description of the absolute energy position of the XAS spectra. We propose here a simple correction scheme for absolute core excitation energies based on auxiliary MOM calculation of lowest core ionization energy. In this work, we used the computationally demanding MP2 and CCSD approaches to calculate the lowest core ionization energies. Core ionization energies can be, however, estimated accurately even within the DFT framework.[89] The OT-RSH TDDFT method with this correction provides accurate XAS on an absolute energy scale, and this combined approach is, therefore, recommended for quantitative simulations of valence X-ray absorption spectra of small- to medium-sized molecules.

■ ASSOCIATED CONTENT

Supporting Information

Errors in absolute excitation energies as a function of the deviation from the IP theorem and the calculated spectra in absolute units. The Supporting Information is available free of charge on the ACS Publications website at DOI: 10.1021/acs.jctc.5b00066.

■ AUTHOR INFORMATION

Corresponding Author

*E-mail: Petr.Slavicek@vscht.cz.

Notes

The authors declare no competing financial interest.

■ ACKNOWLEDGMENTS

Support by the Czech Science Foundation (project no. 13-34168S) is gratefully appreciated. D.H. acknowledges the financial support from specific university research (MSMT No. 20/2015); he is also a student of the International Max Planck Research School "Dynamical Processes in Atoms, Molecules and Solids".

■ REFERENCES

(1) Burke, K.; Werschnik, J.; Gross, E. K. U. *J. Chem. Phys.* **2005**, *123*, 062206.
(2) Casida, M. E.; Huix-Rotllant, M. *Annu. Rev. Phys. Chem.* **2012**, *63*, 287.
(3) Besley, N. A. *Chem. Phys. Lett.* **2004**, *390*, 124.
(4) Dreuw, A.; Head-Gordon, M. *Chem. Rev.* **2005**, *105*, 4009.
(5) Jacquemin, D.; Mennucci, B.; Adamo, C. *Phys. Chem. Chem. Phys.* **2011**, *13*, 16987.
(6) Adamo, C.; Jacquemin, D. *Chem. Soc. Rev.* **2013**, *42*, 845.
(7) Stener, M.; Fronzoni, G.; de Simone, M. *Chem. Phys. Lett.* **2003**, *373*, 115.
(8) George, S. D.; Petrenko, T.; Neese, F. *Inorg. Chim. Acta* **2008**, *361*, 965.
(9) Tsuchimochi, T.; Kobayashi, M.; Nakata, A.; Imamura, Y.; Nakai, H. *J. Comput. Chem.* **2008**, *29*, 2311.

DOI: 10.1021/acs.jctc.5b00066
J. Chem. Theory Comput. XXXX, XXX, XXX−XXX

(10) Besley, N. A.; Asmuruf, F. A. *Phys. Chem. Chem. Phys.* **2010**, *12*, 12024.
(11) Laurent, A. D.; Jacquemin, D. *Int. J. Quantum Chem.* **2013**, *113*, 2019.
(12) Nakata, A.; Imamura, Y.; Otsuka, T.; Nakai, H. *J. Chem. Phys.* **2006**, *124*, 094105.
(13) Nakata, A.; Imamura, Y.; Nakai, H. *J. Chem. Phys.* **2006**, *125*, 064109.
(14) Imamura, Y.; Nakai, H. *Chem. Phys. Lett.* **2006**, *419*, 297−303.
(15) Song, J.-W.; Watson, M. A.; Nakata, A.; Hirao, K. *J. Chem. Phys.* **2008**, *129*, 184113.
(16) Song, J.-W.; Watson, M. A.; Hirao, K. *J. Chem. Phys.* **2009**, *131*, 144108.
(17) Besley, N. A.; Peach, M. J. G.; Tozer, D. J. *Phys. Chem. Chem. Phys.* **2009**, *11*, 10350.
(18) Cai, Z.-L.; Sendt, K.; Reimers, J. R. *J. Chem. Phys.* **2002**, *117*, 5543.
(19) Dreuw, A.; Head-Gordon, M. *J. Am. Chem. Soc.* **2004**, *126*, 4007.
(20) Tozer, D. J.; Handy, N. C. *J. Chem. Phys.* **1998**, *109*, 10180.
(21) Perdew, J. P.; Zunger, A. *Phys. Rev. B* **1981**, *23*, 5048.
(22) Mori-Sánchez, P.; Cohen, A. J.; Yang, W. *J. Chem. Phys.* **2006**, *125*, 201102.
(23) Becke, A. D. *J. Chem. Phys.* **1993**, *98*, 1372.
(24) Leininger, T.; Stoll, H.; Werner, H.-J.; Savin, A. *Chem. Phys. Lett.* **1997**, *275*, 151.
(25) Heyd, J.; Scuseria, G. E.; Ernzerhof, M. *J. Chem. Phys.* **2003**, *118*, 8207.
(26) Yanai, T.; Tew, D. P.; Handy, N. C. *Chem. Phys. Lett.* **2004**, *393*, 51.
(27) Tsuneda, T.; Hirao, K. *Wiley Interdiscip. Rev.: Comput. Mol. Sci.* **2013**, *4*, 375.
(28) Tsuneda, T.; Hirao, K. J. *Chem. Phys.* **2014**, *140*, 18A513.
(29) Tu, G.; Rinkevicius, Z.; Vahtras, O.; Ågren, H.; Ekström, U.; Norman, P.; Carravetta, V. *Phys. Rev. A* **2007**, *76*, 022506.
(30) Tu, G.; Carravetta, V.; Vahtras, O.; Ågren, H. *J. Chem. Phys.* **2007**, *127*, 174110.
(31) Imamura, Y.; Nakai, H. *Int. J. Quantum Chem.* **2007**, *107*, 23−29.
(32) Baer, R.; Livshits, E.; Salzner, U. *Annu. Rev. Phys. Chem.* **2010**, *61*, 85.
(33) Vydrov, O. A.; Heyd, J.; Krukau, A. V.; Scuseria, G. E. *J. Chem. Phys.* **2006**, *125*, 074106.
(34) Levy, M.; Perdew, J. P.; Sahni, V. *Phys. Rev. A* **1984**, *30*, 2745.
(35) Almbladh, C.-O.; von Barth, U. *Phys. Rev. B* **1985**, *31*, 3231.
(36) Perdew, J. P.; Levy, M. *Phys. Rev. B* **1997**, *56*, 16021.
(37) Salzner, U.; Baer, R. *J. Chem. Phys.* **2009**, *131*, 231101.
(38) Stein, T.; Kronik, L.; Baer, R. *J. Am. Chem. Soc.* **2009**, *131*, 2818.
(39) Egger, D. A.; Weissman, S.; Refaely-Abramson, S.; Sharifzadeh, S.; Dauth, M.; Baer, R.; Kümmel, S.; Neaton, J. B.; Zojer, E.; Kronik, L. *J. Chem. Theory Comput.* **2014**, *10*, 1934−1952.
(40) Autschbach, J.; Srebro, M. *Acc. Chem. Res.* **2014**, *47*, 25922602.
(41) Garza, A. J.; Osman, O. I.; Asiri, A. M.; Scuseria, G. E. *J. Phys. Chem. B* **2015**, *119*, 1202−1212.
(42) Garrett, K.; Vazquez, X. A. S.; Egri, S. B.; Wilmer, J.; Johnson, L. E.; Robinson, B. H.; Isborn, C. M. *J. Chem. Theory Comput.* **2014**, *10*, 3821−3831.
(43) Kümmel, S.; Kronik, L. *Rev. Mod. Phys.* **2008**, *80*, 3−60.
(44) Imamura, Y.; Kobayashi, R.; Nakai, H. *Int. J. Quantum Chem.* **2013**, *113*, 245.
(45) Moore, B.; Charaf-Eddin, A.; Planchat, A.; Adamo, C.; Autschbach, J.; Jacquemin, D. *J. Chem. Theory Comput.* **2014**, *10*, 4599−4608.
(46) Chakravarty, C. *Int. Rev. Phys. Chem.* **1997**, *16*, 421−444.
(47) Lee, S. Y.; Brown, R. C.; Heller, E. J. *J. Phys. Chem.* **1983**, *87*, 2045.
(48) Ončák, M.; Šištík, L.; Slavíček, P. *J. Chem. Phys.* **2010**, *133*, 174303.
(49) Sala, F. D.; Rousseau, R.; Görling, A.; Marx, D. *Phys. Rev. Lett.* **2004**, *92*, 183401.
(50) Leetmaa, M.; Ljungberg, M.; Lyubartsev, A.; Nilsson, A.; Pettersson, L. *J. Electron Spectrosc. Relat. Phenom.* **2010**, *177*, 135−157.
(51) Schwartz, C. P.; Uejio, J. S.; Saykally, R. J.; Prendergast, D. *J. Chem. Phys.* **2009**, *130*, 184109.
(52) Eyermann, C. J.; Jolly, W. L. *J. Phys. Chem.* **1983**, *87*, 3080−3082.
(53) Kolczewski, C.; Püttner, R.; Plashkevych, O.; Ågren, H.; Staemmler, V.; Martins, M.; Snell, G.; Schlachter, A. S.; Sant'Anna, M.; Kaindl, G.; Pettersson, L. G. M. *J. Chem. Phys.* **2001**, *115*, 6426−6437.
(54) Neeb, M.; Rubensson, J.-E.; Biermann, M.; Eberhardt, W. *J. Electron Spectrosc. Relat. Phenom.* **1994**, *67*, 261.
(55) Kong, L.; Wu, X.; Car, R. *Phys. Rev. B* **2012**, *86*, 134203.
(56) Ceriotti, M.; Bussi, G.; Parrinello, M. *J. Chem. Theory Comput.* **2010**, *6*, 1170.
(57) Ceriotti, M.; Manolopoulos, D. E.; Parrinello, M. *J. Chem. Phys.* **2011**, *134*, 084104.
(58) Perdew, J. P.; Burke, K.; Ernzerhof, M. *Phys. Rev. Lett.* **1996**, *77*, 3865.
(59) Perdew, J. P.; Burke, K.; Ernzerhof, M. *Phys. Rev. Lett.* **1997**, *78*, 1396.
(60) Dunning, T. H., Jr. *J. Chem. Phys.* **1989**, *90*, 1007.
(61) Kendall, R. A.; Dunning, T. H., Jr.; Harrison, R. J. *J. Chem. Phys.* **1992**, *96*, 6796.
(62) Source code available at: https://github.com/PHOTOX/ABIN.
(63) Frisch, M. J.; et al. *Gaussian 09*, Revision D.01; Gaussian, Inc.: Wallingford, CT, 2013.
(64) Wojdyr, M. *J. Appl. Crystallogr.* **2010**, *43*, 1126−1128.
(65) Hirata, S.; Head-Gordon, M. *Chem. Phys. Lett.* **1999**, *314*, 291.
(66) Baer, R.; Neuhauser, D. *Phys. Rev. Lett.* **2005**, *94*, 043002.
(67) Livshits, E.; Baer, R. *Phys. Chem. Chem. Phys.* **2007**, *9*, 2932.
(68) Johnson, R. D., III, Ed. *NIST Computational Chemistry Comparison and Benchmark Database*; NIST Standard Reference Database Number 101, Release 16a; August, 2013. http://cccbdb.nist.gov/.
(69) Takahashi, O.; Pettersson, L. G. M. *J. Chem. Phys.* **2004**, *121*, 10339.
(70) Krishnan, R.; Binkley, J. S.; Seeger, R.; Pople, J. A. *J. Chem. Phys.* **1980**, *72*, 650.
(71) Clark, T.; Chandrasekhar, J.; Spitznagel, G. W.; Schleyer, P. V. R. *J. Comput. Chem.* **1983**, *4*, 294.
(72) Krylov, A. I.; Gill, P. M. W. *Wiley Interdiscip. Rev.: Comput. Mol. Sci.* **2013**, *3*, 317.
(73) Gilbert, A. T. B.; Besley, N. A.; Gill, P. M. W. *J. Phys. Chem. A* **2008**, *112*, 13164.
(74) Feyereisen, M.; Fitzgerald, G.; Komornicki, A. *Chem. Phys. Lett.* **1993**, *208*, 359.
(75) Epifanovsky, E.; Zuev, D.; Feng, X.; Khistyaev, K.; Shao, Y.; Krylov, A. I. *J. Chem. Phys.* **2013**, *139*, 134105.
(76) Jansen, G.; Hess, B. A. *Phys. Rev. A* **1989**, *39*, 6016.
(77) Saue, T.; Visscher, L.; Jensen, H. J. Aa.; Bast, R. with contributions from Bakken, V.; Dyall, K. G.; Dubillard, S.; Ekström, U.; Eliav, E.; Enevoldsen, T.; Fleig, T.; Fossgaard, O.; Gomes, A. S. P.; Helgaker, T.; Laerdahl, J. K.; Lee, Y. S.; Henriksson, J.; Iliaš, M.; Jacob, Ch. R.; Knecht, S.; Komorovský, S.; Kullie, O.; Larsen, C. V.; Nataraj, H. S.; Norman, P.; Olejniczak, G.; Olsen, J.; Park, Y. C.; Pedersen, J. K.; Pernpointner, M.; Ruud, K.; Sałek, P.; Schimmelpfennig, B.; Sikkema, J.; Thorvaldsen, A. J.; Thyssen, J.; van Stralen, J.; Villaume, S.; Visser, O.; Winther, T.; Yamamoto, S. *DIRAC: A Relativistic Ab Initio Electronic Structure Program*, Release DIRAC12; 2012. http://www.diracprogram.org.
(78) Schirmer, J.; Trofimov, A. B.; Randall, K. J.; Feldhaus, J.; Bradshaw, A. M.; Ma, Y.; Chen, C. T.; Sette, F. *Phys. Rev. A* **1993**, *47*, 1136.
(79) Hitchcock, A.; Ishii, I. *J. Electron Spectrosc. Relat. Phenom.* **1987**, *42*, 11−26.
(80) Rühl, E.; Hitchcock, A. P. *Chem. Phys.* **1991**, *154*, 323.
(81) Hitchcock, A. P. *Phys. Scr.* **1990**, *T31*, 159.
(82) Ishii, I.; McLaren, R.; Hitchcock, A. P.; Jordan, K. D.; Choi, Y.; Robin, M. B. *Can. J. Chem.* **1988**, *66*, 2104−2121.
(83) Urquhart, S. G.; Gillies, R. *J. Phys. Chem. A* **2005**, *109*, 2151.
(84) Hitchcock, A. P.; Brion, C. E. *J. Electron Spectrosc. Relat. Phenom.* **1977**, *10*, 317.

DOI: 10.1021/acs.jctc.5b00066
J. Chem. Theory Comput. XXXX, XXX, XXX−XXX

(85) Tamblyn, I.; Refaely-Abramson, S.; Neaton, J. B.; Kronik, L. *J. Phys. Chem. Lett.* **2014**, *5*, 2734−2741.
(86) Hitchcock, A.; Pocock, M.; Brion, C. *Chem. Phys. Lett.* **1977**, *49*, 125−128.
(87) Besley, N. A.; Gilbert, A. T. B.; Gill, P. M. W. *J. Chem. Phys.* **2009**, *130*, 124308.
(88) Tozer, D.; Handy, N. *Phys. Chem. Chem. Phys.* **2000**, *2*, 2117−2121.
(89) Tolbatov, I.; Chipman, D. M. *Theor. Chem. Acc.* **2014**, *133*, 1473.

DOI: 10.1021/acs.jctc.5b00066
J. Chem. Theory Comput. XXXX, XXX, XXX−XXX